A Human–Robot Co-Manipulation Approach Based on Human Sensorimotor Information

Luka Peternel, Nikos Tsagarakis, and Arash Ajoudani

***Abstract*— This paper aims to improve the interaction and coordination between the human and the robot in cooperative execution of complex, powerful, and dynamic tasks. We propose a novel approach that integrates online information about the human motor function and manipulability properties into the hybrid controller of the assistive robot. Through this human-in-the-loop framework, the robot can adapt to the human motor behavior and provide the appropriate assistive response in different phases of the cooperative task. We experimentally evaluate the proposed approach in two human–robot co-manipulation tasks that require specific complementary behavior from the two agents. Results suggest that the proposed technique, which relies on a minimum degree of task-level pre-programming, can achieve an enhanced physical human–robot interaction performance and deliver appropriate level of assistance to the human operator.**

***Index Terms*— Human-robot interaction, electromyography, service robots, force control, motion control.**

I. Introduction

DURING the past several decades robots have become an irreplaceable part of the industry, as they can surpass the human performance when it comes to carrying heavy loads, executing tasks with high speed and precision, or operating in unreachable/hostile environments. While such robots are traditionally designed to work in protected areas with a very limited intervention of the human operators, a complementary line of research is trying to integrate them into the humans daily lives to closely interact with us and provide service or clinical care. Most prominent examples include: rehabilitation robotics where various robotic mechanism are developed to help rehabilitate persons with specific disabilities, and service robotics where the robots are designed to assist individuals in everyday tasks and scenarios. The latter also represents a very important social perspective, as the robots do not completely replace the humans from the work process, which can help to maintain the sense of purpose of the involved person.

A key requirement for the acceptability of the robots in collaborative applications is the ability to work alongside the humans and adapt to their behaviour and needs. Indeed, most of the effort in this area has been devoted to the development of intermediate interfaces to exploit the high-level component of the human system, which is capable of modelling unstructured environment and adapting to various disturbances, in the cooperative framework. In such a way, the robot can demonstrate appropriate and complementary behaviour in response to the human's supervisory role. Through this shared authority framework, the strong points of both human and the robot can be exploited (e.g., superior physical power of the robot and superior cognitive capabilities of the human).

A widely known example of such an interface is the use of force sensors on the robot side to recognise the objective of the human partner and/or to control the cooperation effort. Due to the simplicity of the underlying mechanism, it has been explored in several applications such as collaborative object transportation [1]–[7], object lifting [8], object placing [4], [9], object swinging [10], [11] and posture assistance [12], [13]. Nevertheless, collaborative tasks that involve simultaneous interaction with a rough or uncertain environment (e.g. co-manipulative tool-use) can induce various unpredictable force components to the force sensor reading [14]. In this case, it can be difficult to distinguish the components related to the human behaviour from the ones generated from the interaction with the environment.

Alternatively, visual feedback [6] or language commands [15] can be used to determine the human intention and generate the desired trajectory for the robot controller. However, in some cases the task complexity could potentially prevent the robot from deriving the desired sensorimotor behaviour from these higher-level modalities. Bio-signals such as electromyography (EMG) and electroencephalography (EEG) have also been widely used to account for the human intention in a collaborative setup. In particular, due to the adaptability and ease-of-use of EMG measurements, they have found a wide range of applications in human-in-the-loop robot control such as: prosthesis [16]–[20], exoskeleton [21]–[23] and industrial manipulator control [14], [24], [25]. Another option to obtain the desired collaborative robot behaviour directly on a sensorimotor level is to use robot learning techniques such as: gradual mutual adaptation [12], [23], reinforcement learning [11] or human demonstration [8], [14], [26]–[28].

As regards to the robot's autonomous manipulation capabilities in a collaborative setup, it must be able to stably interact with the unstructured and unpredictable environment. Inspired by the superior physical interaction capabilities of

Manuscript received April 14, 2016; revised October 13, 2016; accepted April 11, 2017. Date of publication April 17, 2017; date of current version August 6, 2017. This work was supported in part by the EC H2020 Project CogIMon under Grant ICT-23-2014, 644727. *(Corresponding author: Luka Peternel.)*

The authors are with the Human–Robot Interfaces and Physical Interaction Laboratory, Istituto Italiano di Tecnologia, 16163 Genova, Italy, and also with the Humanoid Design and Human Centered Mechatronics Lab, Department of Advanced Robotics, Istituto Italiano di Tecnologia, 16163 Genova, Italy (e-mail: luka.peternel@iit.it; nikos.tsagarakis@iit.it; arash.ajoudani@iit.it).

Digital Object Identifier 10.1109/TNSRE.2017.2694553

the humans [29]–[32], such a versatility can be achieved in robots using the impedance control approach that implements virtual mass-spring-damper systems on the contact points with a desired dynamic response [33], [34]. In relatively simple tasks, the parameters of this system can be predefined and kept fixed. However, in more complex tasks or in case where the environment or the task is subject to variations or dynamic uncertainties, the desired response of the robot must be adaptively regulated though the impedance parameters [14], [25], [35]–[38].

In this direction, a recent work exploited the concept of tele-impedance control[1] in a robot learning approach, where the demonstrator could teach the robotic arm how to cooperate with a human partner for co-manipulative tool-use [14]. In this approach the demonstrator was teleoperating the robotic arm and controlling its motion and stiffness trajectories, while cooperating with the human. The learnt trajectories were then used by the robot in the autonomous stage in a periodic manner. The execution speed of the robot was adapted by a feedback based on the estimated human partner motion through an adaptive oscillator. This approach can be effective to solve cooperative human-robot co-manipulation, however it requires relatively complex setup and an experienced demonstrator to achieve a good performance.

With an attempt to overcome the limitations of the traditional human-robot collaborative approaches in the execution of dynamic and complex tasks, in this paper we propose a novel framework that exploits EMG and dynamic manipulability measurements of the human arm to provide the robot with the information about the human motor behaviour and task requirements. Through this information, the robot can adapt its behaviour by a phase-dependent regulation of trajectories, force and impedance (e.g. self-complying/stiffening), to provide a human-like complementary assistive response. The task frame of the robot is adaptively regulated using the dynamic manipulability index of the human arm and is integrated into the developed hybrid force-impedance controller of the robot. Through this minimal set of pre-programmed behaviour, the proposed shared authority framework can benefit from the two sides' superior capabilities, i.e. human's supervisory role and robot's physical strength, to accomplish the desired task.

We validate the proposed method with experiments on a real hardware setup composed of KUKA Lightweight Robot and Pisa/IIT Softhand, through two complementary tasks, namely cooperative wood sawing and cooperative bolt screwing/valve turning. The main challenge of the former is that it requires a good coordination between the agents and at the same time involves rough and unpredictable interaction with the environment. The latter is an example of effort-assist task where the robot must provide a larger torque in cooperative rotational motion, while relying on the human's fine manipulation skills in other phases.

The preliminary results of this study were presented at 2016 IEEE/RSJ International Conference on Intelligent Robots and Systems [39]. This paper extends the method formulation and presents novel experiments and results.

[1]Tele-impedance control is an alternative approach to the bilateral teleoperation in which the robot's Cartesian impedance can be regulated in real-time using enriched command channel from the operator [25].

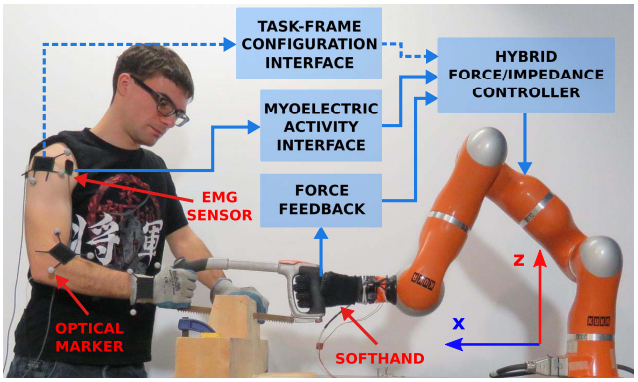

Fig. 1. Human-robot cooperation framework for co-manipulative tasks. The robot is controlled by a hybrid force/impedance controller. The myoelectric activity interface provides the robot controller with human motor behaviour information. Additional task-frame configuration information is based on estimating the force manipulability ellipsoid of human arm endpoint. This interface provides the robot controller with the information about the desired configuration of the task frame. The robot base frame orientation is indicated with arrows.

II. Method

The block scheme of the proposed framework is shown in Fig. 1. The framework is composed of four main units: (1) hybrid force/impedance controller, (2) force feedback unit that provides the necessary feedback for force related tasks, (3) myoelectric activity interface that provides the primary information about the human behaviour and (4) task-frame configuration interface that provides the information about the human-intended task frame configuration.

A. Hybrid Force/Impedance Controller

The main advantage of hybrid force/impedance control scheme is that the robot can regulate force and impedance in certain Cartesian directions as dictated by the task. Previous research [38], [40] has shown clear advantages of the hybrid approach over either pure force or impedance control approach when interaction with an unknown environment is required. For example, using only impedance controller as in the sawing task [14], the robot cannot directly control the contact force. This has to be done indirectly through the control of reference position. If the model of the environment (stiffness properties, etc.) is not known or if it is changing then such control is more difficult.

Based on the advantages, we adopted the hybrid force/impedance control scheme into our approach to establish a desired force between the tool and the environment (through direct force axes), and being able to address the environmental uncertainties while executing the task (through impedance axes). Regarding the sawing task, the desired interaction force/torque in the task reference frame was defined by

$$\boldsymbol{F}_{int} = \boldsymbol{F}_{imp} + \boldsymbol{F}_{for}, \tag{1}$$

where $\boldsymbol{F}_{int}$ is the Cartesian space interaction force/torque acting from the environment on the robot, the term $\boldsymbol{F}_{imp}$ is

related to controlling position task through the impedance, and the term $\boldsymbol{F}_{for}$ is related to the force task, i.e. force control in certain axes, and is meant to ensure the contact between the tool and the environment in those directions. The force F_{imp} related to the impedance was controlled as

$$\boldsymbol{F}_{imp} = \boldsymbol{K}\big(\boldsymbol{x}_a - \boldsymbol{x}_d\big) + \boldsymbol{D}\big(\dot{\boldsymbol{x}}_a - \dot{\boldsymbol{x}}_d\big), \tag{2}$$

where $\boldsymbol{K}$ and $\boldsymbol{D}$ are robot virtual stiffness and damping matrices in Cartesian space, $\boldsymbol{x}_a$ is actual and $\boldsymbol{x}_d$ is reference pose of the robot end-effector. The force $\boldsymbol{F}_{for}$ was controlled by a PID controller based on the measured/estimated force feedback

$$\boldsymbol{F}_{for} = \boldsymbol{K}_P^F \boldsymbol{e}_F + \boldsymbol{K}_D^F \dot{\boldsymbol{e}}_F + \boldsymbol{K}_I^F \int \boldsymbol{e}_F \mathrm{d}t, \tag{3}$$

$$\boldsymbol{e}_F = \boldsymbol{S}_F\big(\boldsymbol{F}_a - \boldsymbol{F}_d\big), \tag{4}$$

where $\boldsymbol{e}_F$ is the error between the actual force $\boldsymbol{F}_a$ and the desired force $\boldsymbol{F}_d$, $\boldsymbol{K}^F$ are gains of PID controller and $\boldsymbol{S}_F$ is a diagonal matrix that is used to select the axes in which the force should be controlled. If the axis is force controlled, the respective diagonal element should be equal to one, otherwise it is set to zero. PID controller was used to compensate for uncertainties such as: environmental disturbances, model and kinematics errors, joint friction, etc. If a simultaneous control of both impedance F_{imp} and force F_{for} is required in the same axis, stability issue might have to be considered. A solution to avoid such issues can be implemented by using the approach proposed in [38].

The desired interaction force $\boldsymbol{F}_{int}$ in Cartesian space was controlled at the robot joint torque level

$$\boldsymbol{M}(\boldsymbol{q})\ddot{\boldsymbol{q}} + \boldsymbol{C}(\boldsymbol{q}, \dot{\boldsymbol{q}})\dot{\boldsymbol{q}} + \boldsymbol{g}(\boldsymbol{q}) = \boldsymbol{\tau} + \boldsymbol{J}_r^T \boldsymbol{F}_{int}, \tag{5}$$

where $\boldsymbol{\tau}$ is a vector of robot joint torques, $\boldsymbol{q}$ is vector of joint angles, $\boldsymbol{J_r}$ is robot arm Jacobian matrix, $\boldsymbol{M}$ is mass matrix, $\boldsymbol{C}$ is Coriolis and centrifugal vector and $\boldsymbol{g}$ is gravity vector. Given that we know the dynamical model of the robot, we can calculate the necessary joint torques $\boldsymbol{\tau}$ to produce the desired interaction force/torque $\boldsymbol{F}_{int}$. The calculated torques $\boldsymbol{\tau}$ were used to control KUKA robotic arm in joint torque control mode.

B. Myoelectic Activity Interface

This modality was developed to enable the robot to replicate an appropriate stiffness increasing/decreasing regulation strategy in our human-robot co-manipulation setup. Previous studies [14], [41] showed that phase-dependent stiffness increasing/decreasing regulation strategy of the human partners in cooperative tasks has been shown to play a very important role in the determination and perception of the leader-follower roles. The end-effector stiffness of the first agent perceived by the second agent can be described as [42][2]

$$\boldsymbol{K}_{c_1}^{(2)} = \boldsymbol{J}_1^{+T}\big(\boldsymbol{K}_{q_1}(\boldsymbol{q}, \boldsymbol{A}) - \boldsymbol{G}_{\boldsymbol{q}}\big)\boldsymbol{J}_1^{+}, \tag{6}$$

$$\boldsymbol{G}_q = \frac{\partial \boldsymbol{J}_1^T \boldsymbol{F}_{ext}}{\partial \boldsymbol{q}} + \frac{\partial \boldsymbol{\tau}_g(\boldsymbol{q})}{\partial \boldsymbol{q}}, \tag{7}$$

[2]Assuming that the the link in-between the two agents is rigid.

where $\boldsymbol{K}_{c_1}^{(2)}$ is Cartesian stiffness matrix of the first agent as perceived by the second agent, $\boldsymbol{J}_1$ is the Jacobian of the first agent's limb, $\boldsymbol{K}_{q_1}(\boldsymbol{q}, \boldsymbol{A})$ is joint stiffness matrix of the first agent, $\boldsymbol{A}$ is muscle activity vector and $\boldsymbol{F}_{ext}$ and $\boldsymbol{\tau}_g(\boldsymbol{q})$ are effects of external load and gravity, respectively.

The above relation suggests that the perceived Cartesian stiffness profile depends on the joint stiffness (through muscular contraction and co-contractions) and the applied external force. One can exploit a complex model of the human arm endpoint stiffness (see [25], [42]) to estimate the volume and the direction of the desired Cartesian stiffness profile. This process requires an off-line identification and calibration phase that will certainly limit the application of the proposed setup, especially in household or industrial settings. In this paper, we break down this problem by tracking the stiffening trend of the human operator using a simplistic approach, while the intended task frame is identified using a more practical method as explained in section II-C.

Measured electromyography (EMG) signals of muscles were first filtered by a 2nd order high-pass filter with cutoff frequency 10 Hz, then rectified and lastly filtered by a 2nd order low-pass filter with cutoff frequency 2.5 Hz. Processed EMG was then normalised using maximal voluntary contraction (MVC) [43], [44]. The mapping between the processed EMG and muscle activation level was defined as

$$0 \leq A_i(t) = \frac{EMG_i(t)}{MVC_i} \leq 1, \tag{8}$$

where A is muscle activation level, $EMG(t)$ is processed EMG signal and MVC is EMG signal under maximal voluntary contraction of the muscle. Subscript number i corresponds to agonist and antagonist muscles of the chosen muscle pair.

The mapping between the muscle activation and joint stiffness trend (c_h) was defined as [19]

$$c_h = b_1 \frac{1 - e^{-b_2(A_1 + A_2)}}{1 + e^{-b_2(A_1 + A_2)}}, \tag{9}$$

where parameter b_1 defines maximum amplitude and b_2 defines the shape and is determined experimentally.[3] The overall representation of the estimated human joint stiffness (9) takes into account the contribution from a single muscle contraction and/or muscle pair co-contraction. The stiffness estimation can be scaled $c_h' = a \cdot c_h$ to a certain operational range of the human stiffness, where factor a is determined experimentally (see section III). Condition $c_h' \in [0\ 1]$ and $c_h \in [0\ 1]$ should be maintained.

We used a simplified single joint stiffness as an estimation of the human arm stiffness in the relevant axis of Cartesian space [42]. It is well-known that stiffening pattern can be observed among different antagonistic pairs of the arm since human arm muscle activations follow a synergistic pattern [46], [47].

The mapping between the estimated human stiffness and robotic arm stiffness modulation parameter was defined as

$$k_r = c_h'(k_{max} - k_{min}) + k_{min}, \tag{10}$$

[3]In case the task operation is within limited muscle activity range (e.g. within 30% of MVC), the linear mapping approximation can be sufficient [45].

where k_{max} and k_{min} determine the range of controllable robot stiffness.

1) Reciprocal Tele-Impedance: If the task is reciprocal in terms of phase of operation, the robot should read the human intention and behave in a reciprocal manner. An example of such task is cooperative sawing. While the first agent is stiff to pull the saw, the second agent must remain compliant not to oppose the effort of the first agent. In the next phase the roles are reversed and the second agents becomes stiff to pull the saw, while the other remains compliant. The stiffness in axis/axes designated for motion control was obtained by

$$\boldsymbol{K}_{ctrl} = \boldsymbol{S}_K\left(1 - k_r\right), \tag{11}$$

where $\boldsymbol{S}_K$ is a diagonal matrix that is used to select the axes in which the stiffness should be modulated (units of the first three elements are N/m, while units of the last three are Nm/rad) and $\boldsymbol{K}_{ctrl}$ is matrix that is used to control the stiffness of the designated axes. If the specific axis should be constant then the respective diagonal element of $\boldsymbol{S}_K$ should be equal zero. The robot Cartesian stiffness used in (2) is equal to

$$\boldsymbol{K} = \boldsymbol{K}_{const} + \boldsymbol{K}_{ctrl}, \tag{12}$$

where $\boldsymbol{K}_{const}$ is a diagonal matrix containing stiffness values of axes that should be constant.

2) Mirrored Tele-Impedance: If the task requires both agents to produce the same behaviour in a certain phase of task operation, the human intention should be mirrored on the robot side. One such example is cooperative bolt screwing or valve turning. When the bolt/valve should be turned, both agents should be stiff to produce the torque in the same direction and perform the rotation. In the next phase, both agents should become complaint to reconfigure and prepare for another rotation cycle. In such case, the human stiffness should be mirrored on the robot as

$$\boldsymbol{K}_{ctrl} = \boldsymbol{S}_K k_r, \tag{13}$$

where $\boldsymbol{K}_{ctrl}$ can be used in (12).

C. Task-Frame Configuration Interface

It is well known that humans exploit the use of arm configurations to achieve a task-appropriate kinematic or dynamic behaviour. Therefore, one basic way to understand the intention of the human cooperator is to observe the pose-related properties, such as velocity and force manipulability measures. These measures provide the information about velocity and force production capacity of the manipulator's end-effector in a certain joint configuration [48].

If motion in a certain axis represents the dominant aspect of the task then the human should adjust its arm configuration in a way that the velocity manipulability can be exploited. On the other hand, if force in a certain axis represents the dominant aspect of the task then the human should adjust its arm configuration in a way that the force manipulability can be exploited. For example in the sawing task, the sawing motion axis requires a force production to pull the saw and drive the blade, which in turn cuts the material. Ideally, the human should align the sawing axis with the highest force manipulability direction to optimise that task execution. The robot counterpart should then adjust its own sawing motion axis to follow the human intention and accommodate the collaborative effort.

In the proposed approach the robot task reference frame (for sawing task) is adjusted based on the estimated human arm endpoint force manipulability ellipsoid. This measure describes the major directions in which the human operator can effectively control the interaction forces. The force manipulability can be derived from

$$\boldsymbol{\tau} = \boldsymbol{J}_h^T \boldsymbol{F}, \tag{14}$$

$$\boldsymbol{\tau}^T \boldsymbol{\tau} = \boldsymbol{F}^T \boldsymbol{J}_h \boldsymbol{J}_h^T \boldsymbol{F} = 1, \tag{15}$$

where $\boldsymbol{J}_h$ is human arm Jacobian matrix, $\boldsymbol{\tau}$ is joint torque vector and $\boldsymbol{F}$ is endpoint force vector.

The endpoint force manipulability ellipsoid can be determined by eigenvalues and eigenvectors of $(\boldsymbol{J}_h \boldsymbol{J}_h^T)^{-1}$. We used eigenvectors to determine the orientation of the task frame in a way that the dominant axis of the force manipulability ellipsoid was aligned with the sawing axis. We selected the sawing axis to be x-axis of the task frame.

To adjust the Cartesian stiffness behaviour to the estimated task frame, we adjusted the stiffness matrix $\boldsymbol{K}_{adj}$ in the robot base frame by

$$\boldsymbol{K}_{adj} = |\boldsymbol{U}_R \cdot \boldsymbol{K}_{eig} \cdot \boldsymbol{V}_R^T|, \tag{16}$$

where $\boldsymbol{K}_{eig}$ is a diagonal matrix containing eigenvalues of stiffness matrix $\boldsymbol{K}$. Matrices $\boldsymbol{U}_R$ and $\boldsymbol{V}_R$ contain left and right singular vectors of $(\boldsymbol{J}_h \boldsymbol{J}_h^T)^{-1}$ and were obtained by singular value decomposition. In addition to adjusting the stiffness matrix, we also controlled the orientation of the robotic hand to correspond to the adjusted task frame. With this, we achieved a more natural operation as that the robotic hand orientation better matched the current orientation of the human hand.

To control the robot Cartesian damping, we based the damping matrix design on *factorisation design* [49]. The damping matrix $\boldsymbol{D}$ was calculated based on the adjusted Cartesian stiffness matrix

$$\boldsymbol{D} = \boldsymbol{\Lambda}_* \boldsymbol{D}_\xi \boldsymbol{K}_{adj*} + \boldsymbol{K}_{adj*} \boldsymbol{D}_\xi \boldsymbol{\Lambda}_*, \tag{17}$$

where $\boldsymbol{D}_\xi$ is a diagonal matrix containing the damping factors ($\xi = 0.7$), $\boldsymbol{K}_{adj*}\boldsymbol{K}_{adj*} = \boldsymbol{K}_{adj}$ and $\boldsymbol{\Lambda}_*\boldsymbol{\Lambda}_* = \boldsymbol{\Lambda}$, where $\boldsymbol{\Lambda}$ is the Cartesian inertia matrix of the robot. In alternative case, the damping matrix can be designed based on *double diagonalisation design* [49], where we similarly use the adjusted stiffness matrix $\boldsymbol{K}_{adj}$ from (16).

III. Experiments

The experimental evaluation of the proposed approach was carried out in two human-robot co-manipulation tasks that require specific complementary behaviour from the two agents. The first part of experiments reports on a two-person sawing task, representing an example of household and daily-life tasks. This task requires a good coordination between the two agents in various phases. In addition, the varying friction between the saw teeth and the material induces a rough and unpredictable interaction with the environment. In the

second part, a collaborative bolt screwing/valve turning task is considered, which is frequently encountered in industrial part-assembly or disaster response scenarios.

A. Two-Person Sawing Task

Generally, a preferable strategy to analyse and solve the two-person sawing task is to split it into two phases. In the *first phase* the human has to pull/push the saw along the blade to dive the saw, while the cooperating robot should stay compliant in the motion axis in order not to oppose the human's effort. Simultaneously, both human and robot should apply some vertical downward force to produce the friction between the saw teeth and the material. When the saw blade reaches the edge, the roles are switched. In the *second phase*, the robot starts to pull/push the saw back toward itself, while the human stays compliant in the motion axis in order not to oppose robot's effort.

The described actions mainly concern sensorimotor aspect of this cooperative task, over which both human and robot have some degree of responsibility. On the other hand, cognitive aspects of the task include position of incision along the beam, orientation of the cut and execution frequency. These elements were completely controlled by the human. In this way, the human could use his/her superior cognitive capability to control the high-level aspects of the tasks and therefore no complex cognitive skill was required on the robot.

The robot's hybrid controller achieved a Cartesian impedance profile along the direction of the sawing motion ($x-y$ plane). The maximum controllable stiffness along the primary motion axis was set to $k_{max} = 1000$ N/m. The minimum robot stiffness was set to $k_{min} = 100$ N/m to mimic the stiffness in human arm when there is no voluntary muscle contractions.[4] The value was determined based on the measured/estimated stiffness values of human subjects in [30] and [50].

The robot end-effector reference position in this axis was predetermined at the point where the saw blade is at the edge on the robot side. In this way, the robot moved the saw to the desired end position in the phase when it was its turn to pull. When the human pulled back, the robot became compliant and allowed the human to move the saw blade to the other edge by permitting to displace the actual position from the preset desired position. The stiffness in axis perpendicular to the primary motion axis in horizontal plane was set to 0 N/m. This allowed the free motion along that axis and provided the human the adaptability to make a cut at any point along the beam. The rotational stiffness was kept constant at a relatively high value $k_{rot} = 250$ Nm/rad in all axes in order to maintain the desired rotational posture.

To ensure the contact between the blade and the wood, the robot produced a force in the vertical axis ($F_d = -5$ N) according to the PID controller described by (3). We experimentally set the proportional gains of controller in z axis to 0.5 and integral gains to 1.0. While we presented PID controller in (3) for generality, we did not use derivative element in our experiments. PI controller is usually preferred over PID when the force reading is noisy, which is the case in our tasks as the tool interacts with a rough environment.

The two-person sawing task requires the agents to produce reciprocal actions in any of the two phases. To control the robot stiffness we used the proposed interface based on human muscle activity described by (10)-(12). For this task, we selected human shoulder joint Deltoid muscle activity to estimate the robot arm stiffness properties, as it has a dominant role in controlling the endpoint stiffness in this specific task [51]. The surface EMG electrodes were placed on Posterior Deltoid and Anterior Deltoid muscles in accordance with SENIAM recommendations [52]. Before the experiments, the subjects performed a MVC procedure for both selected muscles and we used the obtained values in EMG normalisation. Factor a was set experimentally based on the preliminary human-human collaboration trials. We observed an average minimum value of stiffness estimation c_h peaks and determined the stiffness operational range scaling factor as

$$a = \frac{1}{\min\left(\boldsymbol{c}_h^{peaks}(t)\right)}, \tag{18}$$

where $\boldsymbol{c}_h^{peaks}(t)$ are the measured peaks of stiffness estimation.

Three subjects participated in the sawing experiments. Figs. 2 and 3 illustrate the results of this experiment for two subjects. Please refer to accompanying multimedia file for a video of experiments. The first graph shows the estimated human stiffness parameter c_h, while the second graph shows the robot stiffness along the sawing motion axis. The two are reciprocal according to (11). When the human was pulling the saw, the human stiffness increased and the robot stiffness decreased in order to follow the human action. When the human stopped pulling, the robot stiffness increased and consequently the robot began to pull the saw back toward the initial equilibrium point. The motion of the robot end-effector along the sawing axis (in this case aligned with robot base frame x axis) can be observed in the third graph. While the human and robot cooperatively executed the given task, the wood was gradually cut and the vertical robot end-effector position gradually moved downward, as it can be confirmed by measurements in the third graph.

The fourth graph shows the robot force in vertical axis, which is necessary to maintain the contact between the saw teeth and the wood for the cutting. On average, the actual force was close to the desired. While there were deviations from the desired force due to the interaction with a very rough environment and due to some tilting during the practical execution, these non-ideal conditions did not affect the successful performance of the task.

One of the advantages of the proposed approach is its real-time adaptability. The human can arbitrary increase or decrease the frequency of task execution, or even stop the motion and then continue the motion at any point. This behaviour can be observed in the third graph, where the motion frequency was higher in 0-17 seconds period compared to 17-35 seconds period. The human temporary halted the task execution around

[4]This aspect is not necessary. However, we included it to give a more natural feel to the human operator. It also provides some safety aspect, as the human cannot pull the robot too far without any resistance.

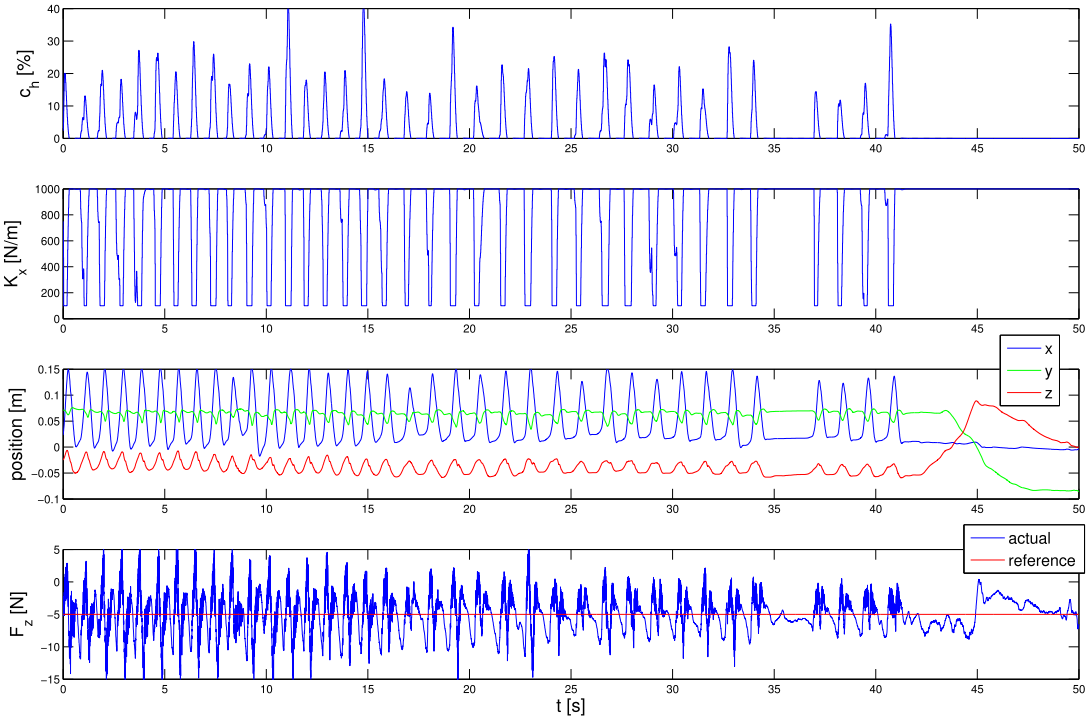

Fig. 2. Results of cooperative human-robot sawing using the proposed control approach. First graph shows the human stiffness estimation. Second graph depicts the robot stiffness along the sawing motion axis. Third graph presents the robot end-effector position along sawing axis (*x*), along beam axis (*y*) and along vertical axis (*z*). Finally, the fourth graph introduces the measured (blue) and reference (red) force along vertical axis.

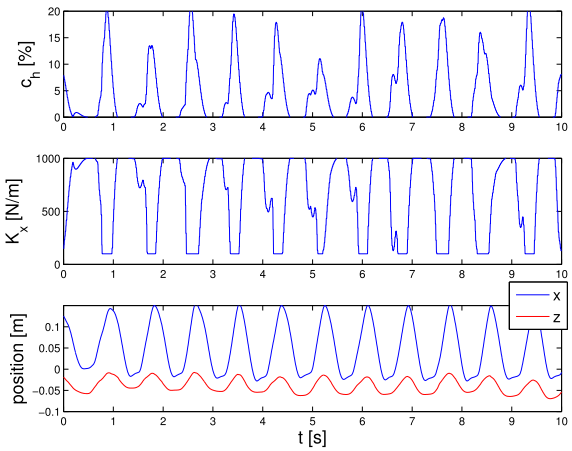

Fig. 3. Results of cooperative human-robot sawing for another subject. The graphs present the same variables as the first three graphs of Fig. 2.

35 seconds and continued it a couple of seconds later. At the end, a new cut was made at a different position along the beam. This can be observed in the third graph by measured robot end-effector position in y axis, which was in this case aligned with the beam of wood.

In the second part of experiment we demonstrated the adaptability of the proposed approach, while varying the orientation of the main cutting motion, using the proposed task-frame configuration interface which is based on the force manipulability ellipsoid of the human arm endpoint. We employed an optical motion capture system (OptiTrack) to measure the kinematics of the human arm and to estimate its Jacobian matrix in real-time [42], [53]. Three optical markers mounted on a flat support base were placed on the shoulder, elbow and wrist joints. In the first stage, the subject was instructed to saw the beam of wood in an orientation aligned with x axis of the robot base frame. In the second stage, the subject was instructed to change the configuration of the task frame so that the sawing was done in an axis that was rotated by approximately 45°. This was done continuously without stopping the setup. Please refer to accompanying multimedia file for a video of the experiment.

Results of this experiment are shown in Fig. 4. The photo and graphs on the left side correspond to the configuration when the task frame was aligned with the robot base frame, while the photo and graphs on the right side correspond to the rotated configuration. First four graphs correspond to the estimated human stiffness c_h, robot stiffness K in x and y axis of the robot base frame, rotation Θ of the task frame around vertical (z) axis and robot motion along task frame x axis (sawing axis), respectively. Each graph shows one periodic cycle of the task. The graphs in the last row show the robot end-effector stiffness ellipsoid[5] in a frame rotated by 180° along z axis with respect to the robot base frame. We present it in this frame for the sake of more evident rotation with respect to the human on the photos. Black dotted lines in the second graph show when each of the stiffness ellipsoid was sampled.

By observing the human stiffness and robot stiffness we can see how the cooperating agents exchanged the pulling and following phases with respect to the motion of the blade. When the blade motion reached the desired peak while the

[5]Since the stiffness in axis perpendicular to sawing motion axis was set to zero, the ellipsoid naturally collapsed into a line in this case. For the sake of generality we still use the term "ellipsoid".

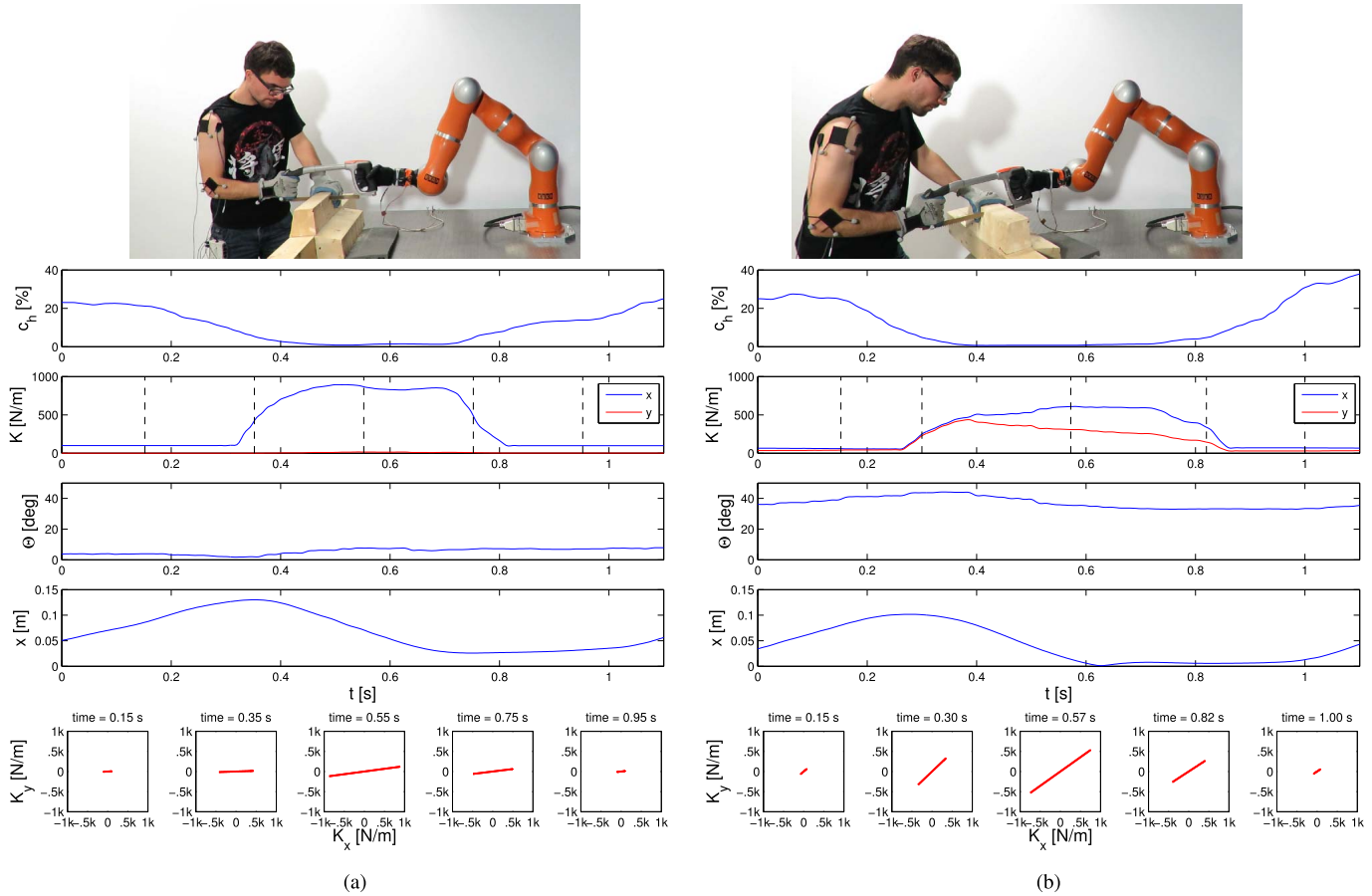

Fig. 4. Result of experiment when using human force manipulability based task-frame configuration interface. Graphs on the left side correspond to a configuration where sawing axis of task frame was aligned with robot base frame *x* axis, while graphs on the left side correspond to configuration where sawing axis of task frame was rotated with respect to the robot base frame. The two photos show different configurations of the task frame. The first graphs show human stiffness estimation. The second graphs show robot end-effector stiffness in *x* and *y* axis of robot base frame. The third graphs show rotation of task frame along *z* axis with respect to robot base frame. Fourth graphs show motion along sawing axis in task frame. The last row graphs show robot stiffness ellipsoids at different phase of the periodic cycle. Black lines in second graphs indicate the moments when they were sampled. (a) Task frame aligned with the robot base frame. (b) Task frame rotated with respect to the robot base frame.

human was pulling, the robot stiffness began to increase and drove the saw back toward itself. Similarly, when the blade motion reached the opposite peak, the human started to pull the saw and the robot became compliant. The stiffness dropped to the prescribed k_{min}, which was used to emulate the passive stiffness of the human muscles.

In the first stage, the task frame was aligned with the robot base frame, therefore stiffness in y axis of the robot base frame was zero. This allowed the human to freely move the saw along the beam of wood to arbitrary choose the desired cutting location. When the wood beam was rotated, a new desired configuration of the task frame was required and the human intuitively adjusted it through the configuration interface. This can be confirmed by observing different angles Θ in left and right graphs. The same can be confirmed by the comparison between the graphs of stiffness ellipsoid, where we can also see how the sawing axis of the ellipsoid scaled with the human stiffness estimation c_h according to (11).

B. Bolt Screwing/Valve Turning Task

The primary action required to screw a bolt or turn a valve is torque production in the axis of rotation. In a cooperative

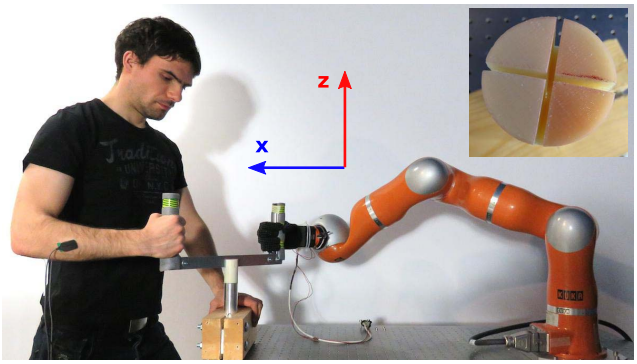

Fig. 5. Experimental setup for collaborative bolt screwing / valve turning. The bolt is turned by a hand-held tool that is inserted into the groove of the bolt head (see upper-right photo for close-up view of the bolt head). The robot base frame orientation is indicated with arrows. In this experiment, the task-frame configuration interface based on human arm end-effector manipulability was not used.

scenario, the partners have to produce the torque in the same direction at the same time to perform the task successfully. In our experiments we used a hand-held tool (see Fig. 5) that the human and the robot had to apply to rotate the bolt. The tool had two handles connected with a metal plate that was inserted into the groove of the bolt head. The strategy

to perform this task was divided into four phases. In the *first phase*, the tool end-effector had to be lowered and inserted into the bolt groove (similar to peg-in-the-hole task). In the *second* phase, the cooperative torque production from both agents was required to turn the bolt for the desired angle. In the *third phase*, the tool had to be lifted outside of the bolt groove. Lastly, in the *fourth phase*, the rotation back to the starting orientation had to be performed in air to prepare for another cycle. The described cycle was then repeated to perform the desired task. The robot detected the switches between the phases by its own sensory system (i.e., positional feedback). Same as in the sawing task, the human took over the main cognitive elements of the task, which include: finding the bolt, positioning the tool to fit into the bolt groove, timing of the motor actions, etc.

For this task we selected human wrist flexor/extensor muscles to extract the human stiffening trend, as they play a major role in the selected bolt turning task. The force applied to the handle of the valve is in the wrist flexor/extensor direction, therefore the joint has to be stabilised by the flexor/extensor muscles to enable the arm to apply the force in that direction at the endpoint [51]. The surface EMG electrodes were placed on Flexor Carpi Radialis and Extensor Carpi Radialis muscles. Before the experiment, we performed MVC procedure for both selected muscles and we used the obtained values for EMG normalisation.

Contrary to the sawing, this task requires the agents to produce mirrored (same) actions in all phases of the task. Instead of using (11), we therefore used the direct form (13) to control the robot cooperative behaviour. In this kind of task, the error between the reference and actual orientation is decreasing as the bolt/valve is turned toward the final rotation. If a constant rotational stiffness is used, the torque gradually decreases with the decreasing orientation error. This might cause issues if the valve friction is either constant (as in our case) or increasing through the turning direction (e.g., closing a valve). To give the human the ability to modulate the torque profile of the robot along the rotational motion, we modified the direct form (13) so that the rotational stiffness can gradually increase when the actual orientation approaches the reference (final) orientation. Therefore, the estimated human stiffness did not directly control the robot stiffness. Instead, the robot stiffness was a time integral of stiffness index

$$\boldsymbol{K}_{ctrl} = \boldsymbol{S}_K k_{int} \int k_r \mathrm{d}t. \tag{19}$$

where k_{int} in integration constant was set experimentally to 1.7 s^{-1} and $\boldsymbol{K}_{ctrl}$ is bounded by the maximum allowable rotational stiffness (set to 19 Nm/rad). To prevent the undesired stiffening due to the small human muscle activity bias, the integration was done only after a predefined threshold was reached. The algorithm (19) was used to control the robot stiffness in both second and fourth phase of the task. The integrated variable $\boldsymbol{K}_{ctrl}$ reset to zero when either fourth-to-first or third-to-fourth phase switches occurred.

An alternative approach to achieve a constant torque over the course of the bolt/valve turn is to use force/torque control part of the hybrid robot controller. However, in our case we preferred impedance control part as the environment is unstructured and the exact required torque is not known. Using high enough stiffness in impedance control makes the robot naturally tend toward the desired final orientation during the rotation of the bolt/valve. By integrating the estimated human effort over time we ensure that, even if the human is not strong the enough to move the tool by itself, the robot effort will eventually increase to a level necessary to perform the task. Another alternative would be to use a constant rotational stiffness, while using the information about human stiffening to gradually move the robot reference orientation in the direction of the turning and therefore gradually turn the bolt/valve. However we preferred the approach with fixed reference orientation as it gives the robot some knowledge of the task. The robot can therefore stops at the desired final orientation even if the human makes some mistakes.

The maximum controllable rotational stiffness of the robot end-effector[6] along the bolt rotation axis (z axis of task frame) was set to 19 Nm/rad, considering the large rotation range that will produce high initiating torque. The minimum controllable stiffness along the same axis was set to 0 Nm/rad. Factor a was set to 1. The rotational stiffness in the other two axes (x and y axis of task frame) were set to a constant value of $k_{rotx} = k_{roty} = 19$ Nm/rad to maintain the desired posture. Translational stiffness in all three axes of task frame were set to $k_x = k_y = k_z = 0$ N/m in order to allow the human partner to freely move the tool in the working area and let the task constraints dominate the movement of the robot even if no trajectories were defined at joint or Cartesian coordinates. In addition, force control was applied in z axis to press down on the bolt with a reference force as in the sawing task. The robot reference rotation along the bolt axis (z axis) was set to $-45°$ for the second phase of the task cycle. This made the robot rotate the tool/bolt from the initial rotation (45°) to the final rotation (-45°) and comply with the human partner when they produced a collaborative effort.

In the fourth phase of the task cycle we designed an automatic algorithm that set the robot rotational reference along the bolt axis to 45° in order to move the tool back into the initial orientation and prepare for another cycle. At the same time, the reference x and y positions were set to the last measured position before entering the fourth phase and translational stiffness k_x and k_y were temporarily increased to a constant value of 300 N/m. This ensured that the tool was stabilised while the rotation was performed in the air. Additionally, the force control in z axis was temporarily suspended so that the robot did not press downward during this phase. The robot entered the forth phase based on the positional feedback from the robot sensory system. The transition was defined by reaching a threshold in z axis above the bolt (i.e. when the human partner moved the tool/robot). The above-mentioned state transition was defined as

$$\boldsymbol{K} = \begin{cases} \boldsymbol{K}_{const} + \boldsymbol{K}_{ctrl} \quad \text{from (12)} & \text{if } z < (z_{th} - z_{hist}) \\ \mathrm{diag}(k_x, k_y, 0, k_{rotx}, k_{roty}, k_{rotz}) & \text{if } z > z_{th}, \end{cases} \tag{20}$$

[6]The robot end-effector is considered at the tool end-effector

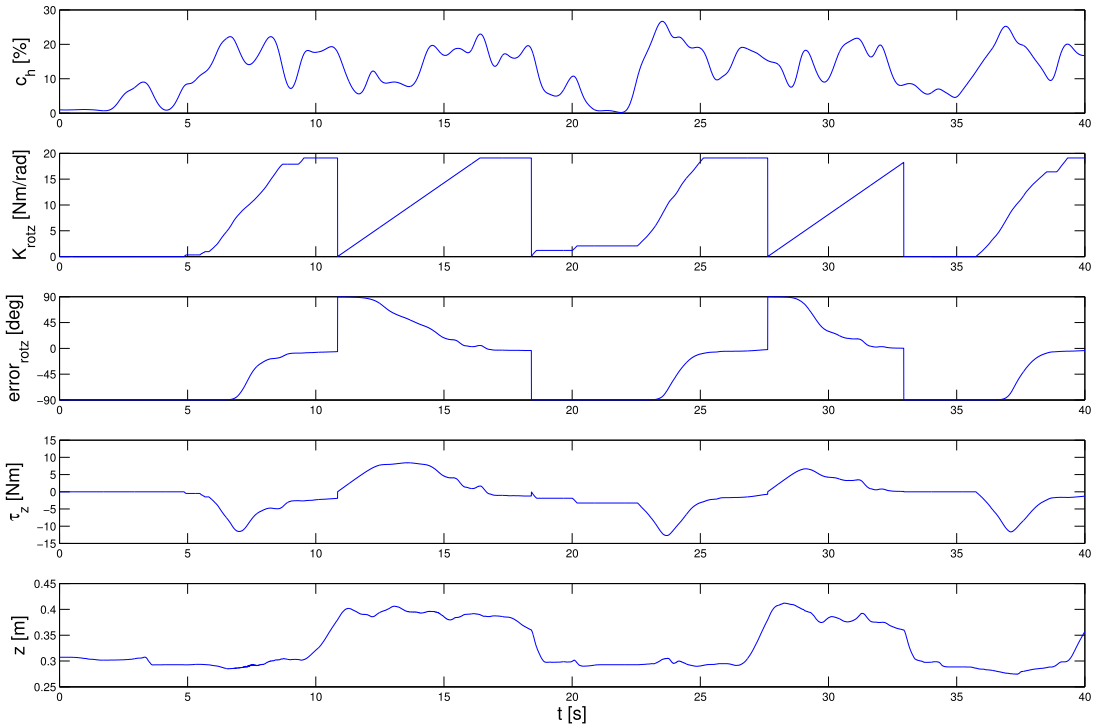

Fig. 6. Results of cooperative human-robot bolt turning using the proposed control approach. The first graph shows the human stiffness estimation. The second graph depicts the robot rotational stiffness in bolt (*z*) axis. The third graph presents the robot/tool orientation error along *z* axis (i.e., difference between reference and actual). The fourth graph indicates the robot assistive torque in *z* axis. Finally, the fifth graph introduces the measured robot/tool end-effector position in *z* axis.

where z_{th} is the threshold that switches between the phases and z_{hist} is a small hysteresis margin that prevents undesired rapid switches. We set z_{th} to 0.08 m above the bolt and $z_{hist} =$ 0.02 m. The constant temporary stiffness parameters for fourth phase state were set for this experiment as $k_x = k_y = 300$ N/m, while k_{rotx}, k_{roty} and k_{rotz} remained unchanged.

For the video of experiments please refer to the accompanying multimedia file. Results of the bolt turning experiments are presented in Fig. 6. The first graph shows the estimated human stiffness index. The second graph shows the robot stiffness as a result of human stiffening patterns obtained by (19). We can see that when the human produced an effort to turn the bolt, the robot started to increase the stiffness to produce the assistive torque and rotate the bolt toward the desired final rotation. The rotation of the bolt can be observed in the third graph where we plotted the rotation error between the actual and reference robot orientation.

The robot assistive torque in the bolt (z) axis is shown in the fourth graph. When the human intended to turn the bolt, the robot torque started to increase and reached the peak when the bolt stiction had to be compensated. We can see that the human exploited the power of the robot to perform the task. On the other hand, the human controlled the cognitive aspects of the task during the task cycles, such as: transitions between the phases of the task, finding the bolt head, insertion of the tool, etc. One of these aspects is evident in the fifth graph, which shows the robot end-effector position in the vertical (z) axis. When the tool had to be inserted into the bolt grove, the position in z axis was lowered as the human appropriately moved the tool/robot. When the tool had to be lifted and rotated back into the orientation suitable for another round, the position in z axis was increased as the human appropriately moved the tool/robot.

IV. Discussion

The proposed approach relies on shared authority between the human and the robot and exploits the advantages of each agent. The robot can take over the large portion of the physical aspect (i.e., providing the assistive power beyond human's physical capabilities), while the human uses its superior cognitive capabilities to supervise the execution of the cooperative task.

The main advantage of the proposed method, compared to classic robot programming approach, is that it relies only on a moderate degree of pre-programming. Instead of designing joint-level or Cartesian trajectories, an appropriate definition of the hybrid controller parameters can lead to the generation of desired task motion/force trajectories along the dictated task constraints (e.g. pulling movement of the robot and the rotational torque along the valve in the sawing and bolt-turning experiments, respectively). However, several parameters of the proposed method still have to be predetermined and pre-programmed. In particular, hybrid force/impedance controller definition (references, etc.), maximum and minimum stiffness in (10) and constant stiffness matrix in (11) and (20) depend on the type of the task.

This approach contributed to the enhanced adaptability and intuitiveness of the proposed human-robot interface,

since several task parameters (frequency of the execution, task interruption, etc.) can be varied online, with no need to change the parameters, trajectories, etc.. This is a notable advantage compared to more complex approaches that use adaptive oscillators to periodically repeat the learnt trajectories [14].

The myoelectric activity interface within the proposed framework alone can provide some meaningful information in some co-manipulative tasks. The applicability of the proposed method can be further increased by the recent development of affordable and easy-to-use EMG systems. While the exact estimation of the human impedance and motor behaviour requires measurement of multiple muscles in the arm [25], it has been shown that simplified estimations based on the measurement of fewer muscles can provide sufficient practical results [14], [42].

When using the simplified estimation, different muscles might have to be considered for the myoelectric activity interface to achieve a better performance. If sawing is done in a natural way, i.e. when the sawing axis is in horizontal plane and aligned with forearm, anterior and posterior Deltoid should be sufficient for these configurations as they are involved in the sawing action due to the shoulder flexion/extension [51], [52]. In case of valve turning, when using pole-like handle (as in our experiment), the wrist flexor/extensor muscle are necessary for stabilising the wrist joint during the turning action [51]. However, if the valve has a ring-like handle then wrist abductor/adductor muscles might provide a better estimation. Other tasks may require considering other muscle groups.

If additional complexity is affordable, the proposed task-frame configuration interface can be integrated into the framework to enhance the adaptability of the approach. Affordable and portable tracking devices such as MS Kinect can potentially contribute to the applicability and ease-of-use of the proposed framework in a home or industrial setup.

We examined two main types of co-manipulation task that require either reciprocal or mirrored behaviour between the involved agents. Sawing is an example of reciprocal behaviour and valve/bolt turning is an example of mirrored behaviour. A potential third major example would be heavy object transportation [1]–[7], which inherits some aspects of mirrored behaviour. For example, when the agents have to lift a heavy object together, they both have to produce the force in the same direction at the same time. Or if they have to rotate a heavy object on the ground, they have to produce the torque in the same direction and at the same time.

The method was primarily validated and evaluated qualitatively. Quantitative evaluation can be done through some performance index of the task execution. In case of sawing, the main objective is to cut the wood. This objective can be achieved with different speed, which is generally a good index of task performance. The estimated average speed of woodcutting in z-axis for each subject was: 1.23, 1.51 and 1.38 mm/s. However, the speed is primarily subject dependent and the proposed method adapts to the individual subject based on their behaviour. In this respect, the performance index can primarily give an evaluation of the operator (with respect to the task) and not the proposed robot control method.

Shared interaction forces between the human and the robot could provide some additional insight into the co-manipulation performance [54]. However, the main problem with the co-manipulation is that the human and the robot are physically coupled through a tool or an object and the exact contribution of each agent is difficult to estimate, as the force sensor measures the net force on the tool. In particular, the rough stochastic interaction of tool with the environment (e.g., sawing task) makes such estimation even more difficult as it induces unpredictable forces into the measurement.

In the experiments, the stiffness matrix scaling was performed with frequency up to 1 Hz and amplitude 900 N/m without observing any stability issues. The stiffness matrix configuration changes were performed with frequency up to 0.25 Hz without observing any stability issues. These changes were mostly continuous and were part of the normal operation and task execution. On the other hand, there is a potential stability issue when it comes to sudden discrete changes that may be part of equipment failure (sEMG electrode detachment, motion capture system failure etc.). However, these situations are not expected in the normal operation and should be and were handled by a low-level safety software/hardware modules.

V. Conclusion

In this paper, we proposed a novel method for robot-assisted co-manipulation based on real-time human sensorimotor information. To provide the robot with the information about the human behaviour and intention, a multi-modal human-robot interface was implemented using EMG and force manipulability measurements of the human arm. The proposed method was validated experimentally where the intuitiveness and effectiveness of the approach in successful coordination of two counterparts were evaluated.

Acknowledgment

The authors would like to thank Cheng Fang for providing algorithm for human arm Jacobian calculation.

References

[1] R. Ikeura and H. Inooka, "Variable impedance control of a robot for cooperation with a human," in *Proc. IEEE Intl. Conf. Robot. Autom. (ICRA)*, vol. 3. May 1995, pp. 3097–3102.

[2] K. Kosuge and N. Kazamura, "Control of a robot handling an object in cooperation with a human," in *Proc. 6th IEEE Int. Workshop Robot Human Commun. (RO-MAN)*, Sep. 1997, pp. 142–147.

[3] O. M. Al-Jarrah and Y. F. Zheng, "Arm-manipulator coordination for load sharing using reflexive motion control," in *Proc. IEEE Int. Conf. Robot. Autom.*, vol. 3. Apr. 1997, pp. 2326–2331.

[4] T. Tsumugiwa, R. Yokogawa, and K. Hara, "Variable impedance control with virtual stiffness for human-robot cooperative peg-in-hole task," in *Proc. IEEE/RSJ Int. Conf. Intell. Robots Syst. (IROS)*, vol. 2. Oct. 2002, pp. 1075–1081.

[5] V. Duchaine and C. M. Gosselin, "General model of human-robot cooperation using a novel velocity based variable impedance control," in *Proc. 2rd Joint Eurohaptics Conf. Symp. Haptic Int. Virtual Environ. Teleoper. Syst.*, Mar. 2007, pp. 446–451.

[6] D. J. Agravante, A. Cherubini, A. Bussy, P. Gergondet, and A. Kheddar, "Collaborative human-humanoid carrying using vision and haptic sensing," in *Proc. IEEE Int. Conf. Robot. Autom. (ICRA)*, May 2014, pp. 607–612.

[7] E. Gribovskaya, A. Kheddar, and A. Billard, "Motion learning and adaptive impedance for robot control during physical interaction with humans," in *Proc. IEEE Int. Conf. Robot. Autom. (ICRA)*, May 2011, pp. 4326–4332.

[8] P. Evrard, E. Gribovskaya, S. Calinon, A. Billard, and A. Kheddar, "Teaching physical collaborative tasks: Object-lifting case study with a humanoid," in *Proc. IEEE-RAS Int. Conf. Humanoid Robots*, Dec. 2009, pp. 399–404.

[9] A. Gams, B. Nemec, A. J. Ijspeert, and A. Ude, "Coupling movement primitives: Interaction with the environment and bimanual tasks," *IEEE Trans. Robot.*, vol. 30, no. 4, pp. 816–830, Aug. 2014.

[10] P. Donner and M. Buss, "Cooperative swinging of complex pendulum-like objects: Experimental evaluation," *IEEE Trans. Robot.*, vol. 32, no. 3, pp. 744–753, Jun. 2016.

[11] I. Palunko, P. Donner, M. Buss, and S. Hirche, "Cooperative suspended object manipulation using reinforcement learning and energy-based control," in *Proc. IEEE/RSJ Int. Conf. Intell. Robots Syst. (IROS)*, Sep. 2014, pp. 885–891.

[12] S. Ikemoto, H. B. Amor, T. Minato, B. Jung, and H. Ishiguro, "Physical human-robot interaction: Mutual learning and adaptation," *IEEE Robot. Autom. Mag.*, vol. 19, no. 4, pp. 24–35, Dec. 2012.

[13] L. Peternel and J. Babič, "Learning of compliant human–robot interaction using full-body haptic interface," *Adv. Robot.*, vol. 27, no. 13, pp. 1003–1012, Jun. 2013.

[14] L. Peternel, T. Petrič, E. Oztop, and J. Babič, "Teaching robots to cooperate with humans in dynamic manipulation tasks based on multi-modal human-in-the-loop approach," *Auto. Robots*, vol. 36, no. 1, pp. 123–136, Jan. 2014.

[15] J. R. Medina, M. Shelley, D. Lee, W. Takano, and S. Hirche, "Towards interactive physical robotic assistance: Parameterizing motion primitives through natural language," in *Proc. IEEE RO-MAN*, Sep. 2012, pp. 1097–1102.

[16] K. A. Farry, I. D. Walker, and R. G. Baraniuk, "Myoelectric teleoperation of a complex robotic hand," *IEEE Trans. Robot. Autom.*, vol. 12, no. 5, pp. 775–788, Oct. 1996.

[17] A. B. Ajiboye and R. F. Weir, "A heuristic fuzzy logic approach to EMG pattern recognition for multifunctional prosthesis control," *IEEE Trans. Neural Syst. Rehabil. Eng.*, vol. 13, no. 3, pp. 280–291, Sep. 2005.

[18] N. Jiang, K. Englehart, and P. Parker, "Extracting simultaneous and proportional neural control information for multiple-DOF prostheses from the surface electromyographic signal," *IEEE Trans. Biomed. Eng.*, vol. 56, no. 4, pp. 1070–1080, Apr. 2009.

[19] A. Ajoudani *et al.*, "Exploring teleimpedance and tactile feedback for intuitive control of the pisa/IIT SoftHand," *IEEE Trans. Haptics*, vol. 7, no. 2, pp. 203–215, Apr. 2014.

[20] D. Farina *et al.*, "The extraction of neural information from the surface EMG for the control of upper-limb prostheses: Emerging avenues and challenges," *IEEE Trans. Neural Syst. Rehabil. Eng.*, vol. 22, no. 4, pp. 797–809, Jul. 2014.

[21] J. Rosen, M. Brand, M. B. Fuchs, and M. Arcan, "A myosignal-based powered exoskeleton system," *IEEE Trans. Syst., Man, Cybern. A, Syst., Humans*, vol. 31, no. 3, pp. 210–222, May 2001.

[22] C. Fleischer and G. Hommel, "A human–exoskeleton interface utilizing electromyography," *IEEE Trans. Robot.*, vol. 24, no. 4, pp. 872–882, Aug. 2008.

[23] L. Peternel, T. Noda, T. Petrič, A. Ude, J. Morimoto, and J. Babič, "Adaptive control of exoskeleton robots for periodic assistive behaviours based on EMG feedback minimisation," *PLoS ONE*, vol. 11, no. 2, p. e0148942, Feb. 2016.

[24] J. Vogel, C. Castellini, and P. van Der Smagt, "EMG-based teleoperation and manipulation with the DLR LWR-III," in *Proc. IEEE/RSJ Int. Conf. Intell. Robots Syst. (IROS)*, Sep. 2011, pp. 672–678.

[25] A. Ajoudani, N. Tsagarakis, and A. Bicchi, "Tele-impedance: Teleoperation with impedance regulation using a body–machine interface," *Int. J. Robot. Res.*, vol. 31, no. 13, pp. 1642–1656, 2012.

[26] M. Lawitzky, J. R. Medina, D. Lee, and S. Hirche, "Feedback motion planning and learning from demonstration in physical robotic assistance: Differences and synergies," in *Proc. IEEE/RSJ Int. Conf. Intell. Robots Syst. (IROS)*, Oct. 2012, pp. 3646–3652.

[27] L. Rozo, D. Bruno, S. Calinon, and D. G. Caldwell, "Learning optimal controllers in human-robot cooperative transportation tasks with position and force constraints," in *Proc. IEEE/RSJ Int. Conf. Intell. Robots Syst. (IROS)*, Oct. 2015, pp. 1024–1030.

[28] G. J. Maeda, G. Neumann, M. Ewerton, R. Lioutikov, O. Kroemer, and J. Peters, "Probabilistic movement primitives for coordination of multiple human–robot collaborative tasks," *Auto. Robots*, vol. 41, no. 3, pp. 593–612, Mar. 2017.

[29] F. A. Mussa-Ivaldi, N. Hogan, and E. Bizzi, "Neural, mechanical, and geometric factors subserving arm posture in humans," *J. Neurosci.*, vol. 5, no. 10, pp. 2732–2743, Oct. 1985.

[30] T. Tsuji, P. G. Morasso, K. Goto, and K. Ito, "Human hand impedance characteristics during maintained posture," *Biol. Cybern.*, vol. 72, no. 6, pp. 475–485, May 1995.

[31] E. Burdet, R. Osu, D. W. Franklin, T. E. Milner, and M. Kawato, "The central nervous system stabilizes unstable dynamics by learning optimal impedance," *Nature*, vol. 414, pp. 446–449, Nov. 2001.

[32] D. W. Franklin, R. Osu, E. Burdet, M. Kawato, and T. E. Milner, "Adaptation to stable and unstable dynamics achieved by combined impedance control and inverse dynamics model," *J. Neurophysiol.*, vol. 90, no. 5, pp. 3270–3282, Nov. 2003.

[33] N. Hogan, "Impedance control: An approach to manipulation: Part II—Implementation," *J. Dyn. Syst. Meas. Control*, vol. 107, no. 1, pp. 8–16, Mar. 1985.

[34] A. Albu-Schäffer, C. O. G. Hirzinger, "A unified passivity-based control framework for position, torque and impedance control of flexible joint robots," *Int. J. Rob. Res.*, vol. 26, no. 1, pp. 23–39, Jan. 2007.

[35] M. Garabini, A. Passaglia, F. Belo, P. Salaris, and A. Bicchi, "Optimality principles in variable stiffness control: The VSA hammer," in *Proc. IEEE/RSJ Int. Conf. Intell. Robots Syst. (IROS)*, Sep. 2011, pp. 3770–3775.

[36] C. Yang, G. Ganesh, S. Haddadin, S. Parusel, A. Albu-Schäffer, and E. Burdet, "Human-like adaptation of force and impedance in stable and unstable interactions," *IEEE Trans. Robot.*, vol. 27, no. 5, pp. 918–930, Oct. 2011.

[37] L. Peternel, T. Petrič, and J. Babič, "Human-in-the-loop approach for teaching robot assembly tasks using impedance control interface," in *Proc. IEEE Int. Conf. Robot. Autom. (ICRA)*, May 2015, pp. 1497–1502.

[38] C. Schindlbeck and S. Haddadin, "Unified passivity-based Cartesian force/impedance control for rigid and flexible joint robots via task-energy tanks," in *Proc. IEEE Int. Conf. Robot. Autom. (ICRA)*, May 2015, pp. 440–447.

[39] L. Peternel, N. Tsagarakis, and A. Ajoudani, "Towards multi-modal intention interfaces for human-robot co-manipulation," in *Proc. IEEE/RSJ Int. Conf. Intell. Robots Syst. (IROS)*, Oct. 2016, pp. 2663–2669.

[40] A. L. P. Ureche, K. Umezawa, Y. Nakamura, and A. Billard, "Task parameterization using continuous constraints extracted from human demonstrations," *IEEE Trans. Robot.*, vol. 31, no. 6, pp. 1458–1471, Dec. 2015.

[41] K. B. Reed and M. A. Peshkin, "Physical collaboration of human-human and human-robot teams," *IEEE Trans. Haptics*, vol. 1, no. 2, pp. 108–120, Jul. 2008.

[42] A. Ajoudani, C. Fang, N. G. Tsagarakis, and A. Bicchi, "A reduced-complexity description of arm endpoint stiffness with applications to teleimpedance control," in *Proc. IEEE/RSJ Int. Conf. Intell. Robots Syst. (IROS)*, Sep. 2015, pp. 1017–1023.

[43] J. F. Yang and D. A. Winter, "Electromyographic amplitude normalization methods: Improving their sensitivity as diagnostic tools in gait analysis," *Arch. Phys. Med. Rehabil.*, vol. 65, no. 9, pp. 517–521, 1984.

[44] C. J. de Luca, "The use of surface electromyography in biomechanics," *J. Appl. Biomech.*, vol. 13, no. 2, pp. 135–163, May 1997.

[45] N. Hogan, "Adaptive control of mechanical impedance by coactivation of antagonist muscles," *IEEE Trans. Autom. Control*, vol. 29, no. 8, pp. 681–690, Aug. 1984.

[46] M. Ison and P. Artemiadis, "The role of muscle synergies in myoelectric control: Trends and challenges for simultaneous multifunction control," *J. Neural Eng.*, vol. 11, no. 5, p. 051001, 2014.

[47] M. T. Turvey, "Action and perception at the level of synergies," *Human Movement Sci.*, vol. 26, no. 4, pp. 657–697, Aug. 2007.

[48] T. Yoshikawa, "Manipulability of robotic mechanisms," *Int. J. Robot. Res.*, vol. 4, no. 2, pp. 3–9, 1985.

[49] A. Albu-Schäffer, C. Ott, U. Frese, and G. Hirzinger, "Cartesian impedance control of redundant robots: Recent results with the DLR-light-weight-arms," in *Proc. IEEE Int. Conf. Robot. Autom. (ICRA)*, vol. 3. Sep. 2003, pp. 3704–3709.

[50] A. Ajoudani, *Transferring Human Impedance Regulation Skills to Robots*. Champ, Switzerland: Springer, 2016.

[51] J. Muscolino, *Kinesiology: The Skeletal System Muscle Function*. Amsterdam, The Netherlands: Elsevier, 2016.

[52] H. J. Hermens *et al.*, *European Recommendations for Surface Electromyography: Results of the SENIAM Project (SENIAM)*. Enschede, The Netherlands: Roessingh Res. Develop., 1999.
[53] X. Ding and C. Fang, "A novel method of motion planning for an anthropomorphic arm based on movement primitives," *IEEE/ASME Trans. Mechatronics*, vol. 18, no. 2, pp. 624–636, Apr. 2013.
[54] G. Ganesh, A. Takagi, R. Osu, T. Yoshioka, M. Kawato, and E. Burdet, "Two is better than one: Physical interactions improve motor performance in humans," *Sci. Rep.*, vol. 4, Jul. 2014, Art. no. 3824.

Luka Peternel received the Ph.D. degree in robotics from the University of Ljubljana, Slovenia, in 2015. He performed his Ph.D. studies with the Department of Automation Bio-Cybernetics and Robotics, Jožef Stefan Institute in Ljubljana, Slovenia, and with the Department of Brain–Robot Interface, ATR Computational Neuroscience Labs, Kyoto, Japan. He is currently a Post-Doctoral Researcher with the Human–Robot Interfaces and Physical Interaction Laboratory of Advanced Robotics, Italian Institute of Technology, Genoa, Italy.

Nikos Tsagarakis received the D.Eng. degree in electrical and computer science engineering from the Polytechnic School of Aristotle University, Greece, in 1995, the M.Sc. degree in control engineering and the Ph.D. degree in robotics from the University of Salford, U.K. in 1997 and 2000, respectively. He is currently the Head of the Humanoid Design and Human Centered Mechatronics Lab, IIT.

Arash Ajoudani received the Ph.D. degree in robotics and automation from the Centro di Ricerca Enrico Piaggio, University of Pisa, and the Advanced Robotics Department, Italian Institute of Technology, Italy, in 2014. He is currently a tenure-track Scientist and the Leader of the Human–Robot Interfaces and Physical Interaction Laboratory, IIT.